

1
2 **A single-crystal neutron diffraction study of wardite,**
3 **NaAl₃(PO₄)₂(OH)₄·2H₂O**
4

5 G. Diego Gatta, Alessandro Guastoni, Oscar Fabelo and Maria Teresa Fernandez-Diaz
6

7 **Running title:** Neutron diffraction study of wardite

8
9 **Abstract, Keywords**

10 **Introduction**

11 **Sample description and occurrence**

12 **Experimental methods**

13 **Results**

14 **Discussion and conclusions**

15 **Acknowledgements**

16 **References**

17 **Figures/Tables**
18
19

20 **Corresponding author: G. Diego GATTA**

21 Dipartimento di Scienze della Terra, Università degli Studi di Milano

22 Via Botticelli 23, I-20133 Milano, Italy

23 Tel. +39 02 503 15607, Fax +39 02 503 15597, E-Mail: diego.gatta@unimi.it
24
25
26

27 *Manuscript submitted to Physics and Chemistry of Minerals*

28 **A single-crystal neutron diffraction study of wardite,**
29 **NaAl₃(PO₄)₂(OH)₄·2H₂O**
30

31 G. Diego Gatta^{1,2}, Alessandro Guastoni³, Oscar Fabelo⁴ and Maria Teresa Fernandez-Diaz⁴
32

33 ¹Dipartimento di Scienze della Terra, Università degli Studi di Milano,
34 Via Botticelli 23, I-20133 Milano, Italy

35 ²CNR-Istituto di Cristallografia, Via Amendola 122/O, I-70126 Bari, Italy

36 ³Dipartimento di Geoscienze, Università degli Studi di Padova,
37 Via G. Gradenigo 6, I-35131, Padova, Italy

38 ⁴Institut Laue-Langevin, 71 Avenue des Martyrs, F-38000 Grenoble, France
39

40
41 **Abstract**

42 The crystal structure and crystal chemistry of wardite, ideally NaAl₃(PO₄)₂(OH)₄·2H₂O, was
43 investigated by single-crystal neutron diffraction (data collected at 20 K) and electron microprobe
44 analysis in wavelength-dispersive mode. The empirical formula of the sample used in this study is:
45 (Na_{0.91}Ca_{0.01})_{Σ=0.92}(Al_{2.97}Fe³⁺_{0.05}Ti_{0.01})_{Σ=3.03}(P_{2.10}O₈)(OH)₄·1.74H₂O. The neutron diffraction data
46 confirm that the crystal structure wardite can be described with a tetragonal symmetry (space group
47 *P*4₁2₁2, *a* = *b* = 7.0577(5) and *c* = 19.0559(5) Å at 20 K) and consists of sheets made by edge-sharing
48 Na-polyhedra and Al-octahedra along with vertex-sharing Al-octahedra, parallel to (001), connected
49 by P-tetrahedra and H-bonds to form a (001) layer-type structure, which well explains the
50 pronounced {001} cleavage of the wardite crystals. The present data show that four
51 crystallographically independent H sites occur into the structure of wardite, two belonging to a H₂O
52 molecule (*i.e.*, H1-O6-H2) and two forming hydroxyl groups (*i.e.*, O5-H3 and O7-H4). The location
53 of the hydrogen atoms allow us to define the extensive network of H-bonds: the H-atoms belonging
54 to the H₂O molecule form strong H-bonds, whereas both the H-atoms belonging to the two
55 independent hydroxyl groups form weak interactions with bifurcated bonding schemes. As shown
56 by the root-mean-square components of the displacement ellipsoids, oxygen and hydrogen atoms
57 have slightly larger anisotropic displacement parameters if compared to the other sites (populated
58 by P, Al and Na). The maximum ratio of the *max* and *min* root-mean-square components of the
59 displacement ellipsoids is observed for the protons of the hydroxyl groups, which experience
60 bifurcated H-bonding schemes. A comparative analysis of the crystal structure of wardite and
61 fluorowardite is also provided.
62

63

64 **Keywords:** Wardite, phosphates, single-crystal neutron diffraction, crystal chemistry, hydrogen
65 bonding.

66

67 **Introduction**

68 Wardite, ideally $\text{NaAl}_3(\text{PO}_4)_2(\text{OH})_4 \cdot 2\text{H}_2\text{O}$, is a hydrous phosphate mineral discovered and
69 described by Davison (1896). It was found in cavities in variscite nodules from the Clay Canyon
70 deposit (near Fairfield) in Utah County (Davison 1896; Kampf et al. 2014). Wardite is a hydrothermal
71 mineral, which occurs in phosphate-rich zones of granite pegmatites. After a series of experiments
72 aimed to describe the chemical nature and the symmetry of the wardite crystals (*e.g.*, Hurlbut 1952;
73 Heritsch 1955), its structure was solved by Fanfani et al. (1970), on the basis of single-crystal X-ray
74 intensity data (collected by Weissenberg method with multiple-film integrated photographs) and using
75 a crystal from the type locality. The authors described the structure of wardite in the space group
76 $P4_12_12$, with unit-cell constants $a = b \sim 7.03 \text{ \AA}$, $c \sim 19.04 \text{ \AA}$ (and $\alpha = \beta = \gamma = 90^\circ$). The wardite
77 structure consists of sheets of Al- and Na-coordination polyhedra sharing vertices and edges. These
78 sheets, parallel to (001), are connected to each other along the [001] direction by PO_4 -tetrahedra (and
79 H-bonds) (Fig. 1). The structure model reported by Fanfani et al. (1970) is consistent, in terms of bond
80 distances and angles of the Na-, Al- and P-polyhedra. However, the quality of the data at that time did
81 not allow the authors to locate the H sites, leaving open questions about configuration of the H_2O
82 molecules and OH-groups and, as a consequence, about the H-bonding scheme in the wardite structure.
83 Wardite contains up to 18 wt% of H_2O , therefore the H-content is not negligible. Based on electrostatic
84 valences balance of the oxygen sites, Fanfani et al. (1970) suggested the potential occurrence of one
85 independent H_2O -molecule and two independent hydroxyl-groups. A series of experiments on wardite
86 have been performed by infrared and Raman spectroscopies (*e.g.*, Breitingner et al. 2004; Frost and
87 Erickson 2005; Frost and Xi 2012). However, the full description of the active modes was hindered by
88 the lack of a structure model in which the H sites positions, their vibrational regimes and the H-
89 bonding scheme were known.

90 More recently, Kampf et al. (2014) reported the occurrence of fluorowardite, ideally
91 $\text{NaAl}_3(\text{PO}_4)_2(\text{OH})_2\text{F}_2 \cdot 2\text{H}_2\text{O}$. The structure was solved and described on the basis of a single-crystal X-
92 ray structure refinement; a comparative description of the crystal structure of wardite and fluorowardite
93 was provided.

94 In the framework of a long-term project on the crystal-chemistry of hydrous phosphates (*e.g.*, Gatta
95 et al. 2013a, 2013b, 2014a, 2014b, 2015), we have reinvestigated the crystal structure and crystal

96 chemistry of wardite by single-crystal neutron diffraction and electron microprobe analysis in
97 wavelength-dispersive mode (EPMA–WDS), in order to provide: *i*) the reliable location of the proton
98 sites and the real topological configuration of the OH-groups and H₂O molecules, for a full description
99 of the atomic relationship via the H-bonds; *ii*) the anisotropic displacement parameters of all the atomic
100 sites, H-sites included. To carry out this objective, single-crystal neutron diffraction data were collected
101 at low temperature (20 K) in order to reduce the thermal displacement of the H-sites.

102

103 **Sample description and occurrence**

104 The sample of wardite used in this study belongs to the collection of the Museum of
105 Mineralogy of the University of Padova (catalogue number MM18662). The hand specimen is a
106 group of pseudo-octahedral gem-quality crystals, formed by nearly equant tetragonal di-pyramids,
107 striated perpendicular to [001], with pale blue-green colour and up to 1 cm in length. The larger
108 crystals are transparent and vitreous. The specimen was collected at the Rapid Creek area, Canada.
109 The Rapid Creek is a remote region in the north-eastern Yukon Territory, but it represents a
110 remarkable deposit of uncommon and rare phosphate mineral species. Since the early 70s, this area
111 became, among mineralogists and mineral collectors, one of the most important sources for fine
112 minerals like arrojadite group minerals, augelite, collinsite, gorceixite, goyazite, kryzhanovskite,
113 lazulite, wardite and whiteite (Robinson et al. 1992). This is also the type locality for several new
114 iron-, magnesium-, manganese- and barium-phosphate minerals, including arrojadite-(KNa) (Moore
115 et al. 1981), barićite (Sturman and Mandarino 1976), garyansellite (Sturman and Dunn 1984),
116 gormanite (Sturman et al. 1981), kulanite (Mandarino and Sturman 1976), penikisite (Mandarino et
117 al. 1977) and rapidcreekite (Roberts et al. 1986), a calcium, hydrate sulphate-carbonate.

118 Young and Roberston (1984) published a geological description of the Rapid Creek area,
119 which is characterized by deposits of siderite and phosphatic ironstone embedded in shales and
120 thick sequences of turbidite sandstones, named Blow River Formation, deposited during the early to
121 mid-Cretaceous. The phosphatic iron formation is composed of phosphate-siderite grains, detrital
122 quartz and skeletal fragments in a matrix of sideritic mudstone. Most of the phosphate grains are not
123 composed by apatite but of rare phosphate minerals including arrojadite, gormanite and satterlyite.
124 At Rapid Creek, well-crystallized phosphates occur within set of rigid fracture which cross-cut the
125 Blow River Formation, where a typical fracture-filling mineral assemblage is related to the
126 composition of the hosting rocks (Robertson 1982). Robertson (1982) identified four major mineral
127 assemblages: 1) Ba-rich set of fractures cross-cutting conglomerates, 2) Ca-rich fractures cross-
128 cutting mudstones, 3) Fe-Mg-Mn rich set of fractures cross-cutting sandstones, and 4) Na-rich set of

129 fractures cross-cutting phosphatic sandstones. The wardite sample used for this study is associate
130 with spheroidal aggregates of millimetric greenish-bluish gormanite and rhombohedral brown
131 vitreous millimetric crystals of siderite, probably related to the type 3 set of fractures as reported by
132 Robertson (1982).

133 There is no geological evidence of the presence of an igneous activity in the area; the host
134 rock is a sedimentary iron-rich formation. Fluid inclusion studies indicate that the sequence of
135 crystallization of phosphates at Rapid Creek occurred between 180-200° C, with quartz, lazulite and
136 arrojadite, which represent the first minerals to crystallize, whilst wardite occurs as late stage
137 phosphate. Except for minor illite and chlorite observed in the shales, no lawsonite, laumontite or
138 pyrophyllite occur in the sedimentary rocks at Rapid Creek (Robertson 1982). For such a reason, the
139 fracture-filling minerals were probably formed in the uppermost diagenesis to the lowermost range
140 of regional metamorphism (Robinson et al. 1992).

141

142 **Experimental methods**

143 Chemical composition of the wardite used in this study was obtained using a CAMECA SX-
144 50 electron microprobe equipped with four wavelength-dispersive spectrometers and one energy-
145 dispersive spectrometer at the laboratory of microanalysis of the Institute for Geosciences and Earth
146 Resources of CNR (Padova). The operating conditions were 20 kV accelerating voltage, 5 nA beam
147 current and 10 µm beam diameter. Counting times were 10 s at the peak and 5 s at the background
148 for major elements, and 20 to 100 s at peak and background for minor elements. X-ray counts were
149 converted into oxide weight percentages using the PAP correction program (Pouchou and Pichoir
150 1991). Calibration was performed using natural and synthetic international standards, in part
151 supplied by Cameca and in part kindly provided by the Smithsonian National Museum of Natural
152 History (Smithsonian Microbeam Standards). The following reference materials, lines, and
153 analysing crystals were used: wollastonite (SiK α -TAP); diopside (CaK α -PET); albite (NaK α -TAP);
154 fluorapatite (PK α -TAP); corundum (AlK α -TAP); MnTiO₃ (TiK α -PET); FeO (FeK α -LIF); MnTiO₃
155 (MnK α -LIF); orthoclase (KK α -PET); AsGa (AsL α , TAP). The elements K and As (and even F)
156 were sought but resulted below the experimental detection limits (*i.e.*, less than 0.03 wt%). Minor
157 evidence of sample dehydration, under the electron beam, were observed. Further details pertaining
158 to the microprobe chemical analysis are given in Table 1.

159 Neutron diffraction data were collected on the four-circle diffractometer D19 at ILL
160 (Grenoble, France) with Cu(331)-monochromated radiation (take-off angle $2\theta_M = 70^\circ$), providing
161 neutrons with a wavelength of 0.9460 Å. The sample was glued on a $\phi = 0.5$ mm vanadium pin

162 and placed on a close-circuit displacer device operated at 20.0(5) K (Archer and Lehmann 1986).
163 The measurement strategy consists of omega (ω) scans of 64 or 79° with steps of 0.07° at different
164 χ and φ positions. A total of 25 ω -scans were collected to complete almost half-Ewald sphere. The
165 Multi-Detector Acquisition Data Software (MAD) from ILL was used for data collection. The unit-
166 cell determination was done by using PFINd and DIRAX programs (Duisenberg 1992). The
167 integration of the raw data and refinement of the UB-matrix, including the off-sets, were done using
168 RETREAT and RAFD19 programs, respectively (Wilkinson et al. 1988). The lattice was found to
169 be metrically tetragonal, and the reflections conditions agreed with the space group $P4_12_12$, as
170 previously reported by Fanfani et al. (1970). A total of 20478 reflections were integrated, out of
171 which 3109 were unique reflections (Laue group $4/mmm$, $R_{\text{int}} = 0.0411$). The absorption correction,
172 mainly due to the hydrogen content of the sample (*ca.* 0.132 mm⁻¹), was carried out using D19abs
173 program (Matthewman et al. 1982). Further details pertaining to the data collection strategy are
174 listed in Table 2 and in Gatta et al. (2018a).

175 Anisotropic crystal-structure refinement based on the neutron intensity data was done in the
176 space group $P4_12_12$ using the SHELXL-2014 software (Sheldrick 2008, 2014), starting from the
177 structure model of Fanfani et al. (1970), without any H atom. The neutron scattering lengths of Na,
178 Al, Fe, P, O and H were taken from Sears (1986). Secondary isotropic extinction effect was
179 corrected according to the formalism of Larson (1967), as implemented in the SHELXL package.
180 Convergence was rapidly reached after the first cycles of refinement with a series of intense
181 negative residual peaks in the final difference-Fourier map of the nuclear density (Fig. 2). Minima
182 in the difference-Fourier maps of the nuclear density showed no evidence of positional or dynamic
183 disorder (Fig. 2). Further cycles of refinement were done with H sites assigned to these peaks (as H
184 has a negative neutron scattering length). At the end of the refinement (with $R_1(F) = 0.0219$ for
185 3106 reflections with $F_o > 4\sigma(F_o)$ and 129 refined parameters), all variable parameters converged
186 with all the principal mean-square atomic displacement parameters positive, including those for the
187 H sites. The variance-covariance matrix showed no significant correlation among the refined
188 variables. Further details pertaining to structure refinement strategy are given in Table 2.
189 Coordinates of the atomic sites and displacement parameters are listed in Tables 3 and 4; selected
190 interatomic distances and angles are given in Table 5.

191

192 **Results and Discussion**

193 The EPMA–WDS analysis of the wardite sample used in this study confirms the general
194 findings previously reported in the literature: the ideal formula of this mineral is

195 $\text{NaAl}_3(\text{PO}_4)_2(\text{OH})_4 \cdot 2\text{H}_2\text{O}$; Na is replaced by a very modest fraction of Ca, P (in tetrahedral
196 coordination) is replaced by a low fraction of Si; Al (in octahedral configuration) is replaced by Fe,
197 Mn and Ti (Table 1). Previous experimental findings confirmed that iron occurs as Fe^{3+} in wardite
198 (Vassilikou-Dova 1993). The empirical formula of wardite used in this study is:
199 $(\text{Na}_{0.91}\text{Ca}_{0.01})_{\Sigma=0.92}(\text{Al}_{2.97}\text{Fe}^{3+}_{0.05}\text{Ti}_{0.01})_{\Sigma=3.03}(\text{P}_{2.10}\text{O}_8)(\text{OH})_4 \cdot 1.74\text{H}_2\text{O}$ (Table 1).

200 The neutron structure refinement of this study, based on intensity data collected at 20 K, is
201 consistent with the general structural model previously obtained by Fanfani et al. (1970), based on
202 single-crystal X-ray intensity data collected at room conditions: wardite structure consists of sheets
203 made by edge-sharing Na-polyhedra (with coordination number = 8) and Al-octahedra along with
204 vertex-sharing Al-octahedra, parallel to (001), connected by P-tetrahedra and H-bonds to form a
205 (001) layer-type structure, which well explains the pronounced {001} cleavage of the wardite
206 crystals (Fig. 1, Table 5). Accordingly, strong structural homologies occur between the crystal
207 structure of wardite and fluorowardite (ideally $\text{NaAl}_3(\text{PO}_4)_2(\text{OH})_2\text{F}_2 \cdot 2\text{H}_2\text{O}$, Kampf et al. 2014). Our
208 data show that in wardite the P-tetrahedron is almost regular (with $\Delta(\text{P-O})_{\text{max}} \sim 0.02 \text{ \AA}$, *i.e.*, the
209 difference between the longest and the shortest bond distances), whereas the two independent Al-
210 octahedra are slightly distorted ($\Delta(\text{Al1-O})_{\text{max}} \sim 0.15 \text{ \AA}$, $\Delta(\text{Al2-O})_{\text{max}} \sim 0.03 \text{ \AA}$). Four
211 crystallographically independent H sites occur into the structure of wardite (namely H1-H4, Table
212 3). In particular:

- 213 - H1 and H2 form a H_2O molecule with the O6 site (oxygen site shared by adjacent Na-
214 polyhedron and Al-octahedron, Fig. 1), with $\text{H1-O6-H2} = 110.0(1)^\circ$, $\text{O6-H1}^* = 1.013 \text{ \AA}$
215 and $\text{O6-H2}^* = 0.996 \text{ \AA}$ (* corrected for *riding motion effect*, Table 5);
- 216 - H3 forms an hydroxyl group with the O5 site (as bridging oxygen site shared by adjacent
217 Al-octahedra, Fig. 1), with $\text{O5-H3}^* = 0.986 \text{ \AA}$ (Table 5);
- 218 - H4 forms an hydroxyl group with the O7 site (as bridging oxygen site shared by adjacent
219 Al-octahedra, Fig. 1), with $\text{O7-H4}^* = 0.989 \text{ \AA}$ (Table 5).

220 The H-bonding scheme in the structure of wardite is now well defined:

- 221 - The H1 site is H-bonded to the O2 site, with $\text{O6-H1}\cdots\text{O2} = 174.4(1)^\circ$ and $\text{H1}\cdots\text{O2} =$
222 $1.617(1) \text{ \AA}$ (Fig. 1, Table 5);
- 223 - The H2 site is H-bonded to the O5 site, with $\text{O6-H2}\cdots\text{O5} = 160.1(1)^\circ$ and $\text{H2}\cdots\text{O5} =$
224 $1.913(1) \text{ \AA}$ (Fig. 1, Table 5);
- 225 - The H3 site shows a bifurcated bonding scheme with $\text{O5-H3}\cdots\text{O1} = 139.9(1)^\circ$ and $\text{H3}\cdots\text{O1}$
226 $= 2.556(1) \text{ \AA}$, and $\text{O5-H3}\cdots\text{O6} = 148.5(1)^\circ$ and $\text{H3}\cdots\text{O6} = 2.347(1) \text{ \AA}$ (Fig. 1, Table 5);

227 - The H4 site also shows a bifurcated bonding scheme with $O7-H4\cdots O3 = 160.5(1)^\circ$ and
228 $H4\cdots O3 = 2.447(1) \text{ \AA}$, and $O7-H4\cdots O4 = 137.9(1)^\circ$ and $H4\cdots O4 = 2.449(1) \text{ \AA}$ (Fig. 1,
229 Table 5).

230 Whereas the H2-O6-H2 molecule experiences two strong H-bonds, as corroborated by the
231 bonding geometry, the two hydroxyl groups show relatively weak interactions (Table 5). The H1-
232 O6-H2 angle (Table 5) is still in the range of the observed H-O-H angles in solid-state materials
233 (Chiari and Ferraris 1982; Steiner 1998 and references therein; Gatta et al. 2008, 2012, 2018b; Lotti
234 et al. 2018). The hydrogen bonds of the H₂O molecule show O-H \cdots O angles $\geq 160^\circ$ (Table 5), with
235 a configuration energetically favorable (*i.e.*, approaching linearity, Steiner 1998); the bifurcated H-
236 bonding configuration of the two independent hydroxyl groups leads to a bonding geometry
237 energetically more costly. In fluorowardite, one of the two independent hydroxyl groups is replaced
238 by fluorine, but the H₂O content is virtually identical to that of wardite: the replacement OH⁻→F⁻ is
239 possible, without any significant rearrangement of the structure, because of the (very) weak H-
240 bonds generated by the hydroxyl group. The H-bonding scheme in the structure of wardite here
241 described is compatible with the findings based on vibrational spectroscopies (*e.g.*, Breitingner et al.
242 2004; Frost and Erickson 2005; Frost and Xi 2012). A more robust description of the active IR
243 vibrational modes, dictated by the H-bonds, can now be delivered on the basis of the experimental
244 findings of this study.

245 As shown by the root-mean-square components of the displacement ellipsoids, oxygen and
246 hydrogen atoms have slightly larger anisotropic displacement parameters if compared to the other
247 sites (populated by P, Al and Na). The maximum ratio of the *max* and *min* root-mean-square
248 components of the displacement ellipsoids is observed for the protons of the hydroxyl groups (*i.e.*,
249 O5-H3 and O7-H4, Table 4), which experience bifurcated H-bonding schemes.

250 The neutron structure refinement does not show evidence of partial site occupancy of the H₂O
251 group (Table 3). In this light, the molecular H₂O fraction of the calculated unit formula (*i.e.*, 1.74
252 molecules *p.f.u.*, Table 1), in which the H₂O wt% was assumed considering (OH)_{Σ=4}, is likely
253 underestimated: according to the neutron structure refinement, wardite contains 2.0 molecules *p.f.u.*.
254 The underestimation of the (total) water content could be related with the replacement of OH-group
255 by fluorine, as observed in fluorowardite, and neither X-ray nor neutron diffraction are able to
256 distinguish unambiguously between O and F as their scattering factors/lengths are quite similar. The
257 EPMA–WDS analysis of the wardite used in this study does not show a significant content of
258 fluorine; however, evidence of dehydration under the electron beam were observed during the
259 EPMA-WDS analysis.

260 **Acknowledgements**

261 The authors thank the Institut Laue-Langevin (Grenoble, France), for the allocation of the beamtime
262 and the Institute for Geosciences and Earth Resources of CNR (Padova) for the microprobe analysis
263 of wardite. Two anonymous reviewers and the Editor, M. Rieder, are thanked. This manuscript is
264 dedicated to Pier Francesco Zanazzi (b. 1939), professor of Mineralogy and Crystallography at the
265 University of Perugia (Italy), who solved and refined the structure of wardite with Luca Fanfani and
266 Antonio Nunzi in the 1970, on the occasion of his 80th birthday.

267

268 **References**

269 Archer J, Lehmann MS (1986) A simple adjustable mount for a two-stage cryorefrigerator
270 on an Eulerian cradle. *J Appl Crystallogr* 19:456-459.

271 Breiting DK, Belz H-H, Hajba L, Komlosi V, Mink J, Brehm G, Colognesi D, Parker SF,
272 Schwab RG (2004) Combined vibrational spectra of natural wardite. *J Molec Struct* 706:95–99.

273 Busing WR, Levy HA (1964) The effect of thermal motion on the estimation of bond lengths
274 from diffraction measurements. *Acta Crystallogr* 17:142-146.

275 Chiari G, Ferraris G (1982) The water molecules in crystalline hydrates studied by neutron
276 diffraction. *Acta Crystallogr B* 38:2331–2341.

277 Davison JM (1896) Wardite: a new hydrous basic phosphate of alumina. *Am J Science*
278 2:154–155.

279 Duisenberg AJM (1992) Indexing in single-crystal diffractometry with an obstinate list of
280 reflections. *J Appl Crystallogr* 25:92-96.

281 Fanfani L, Nunzi A, Zanazzi PF (1970) The crystal structure of wardite. *Mineral Mag*
282 37:598-605.

283 Frost RL, Erickson KL (2005) Near-infrared spectroscopic study of selected hydrated
284 hydroxylated phosphates. *Spectrochim Acta A* 61:45-50.

285 Frost RL, Xi YA (2012) Vibrational spectroscopic study of the phosphate mineral Wardite
286 $\text{NaAl}_3(\text{PO}_4)_2(\text{OH})_4 \cdot 2\text{H}_2\text{O}$. *Spectrochim Acta A* 93:155-163.

287 Gatta GD, Rotiroti N, McIntyre GJ, Guastoni A, Nestola F (2008) New insights into the
288 crystal chemistry of epididymite and eudidymite from Malosa, Malawi: a single-crystal neutron
289 diffraction study. *Am Mineral* 93:1158–1165.

290 Gatta GD, McIntyre GJ, Swanson GJ, Jacobsen SD (2012) Minerals in cement chemistry: a
291 single-crystal neutron diffraction and Raman spectroscopic study of thaumasite,
292 $\text{Ca}_3\text{Si}(\text{OH})_6(\text{CO}_3)(\text{SO}_4) \cdot 12\text{H}_2\text{O}$. *Am Mineral* 97:1060–1069.

293 Gatta GD, Vignola P, Meven M, Rinaldi R (2013a) Neutron diffraction in gemology:
294 Single-crystal diffraction study of brazilianite, $\text{NaAl}_3(\text{PO}_4)_2(\text{OH})_4$. *Am Mineral* 98:1624–1630.

295 Gatta GD, Nénert G, Vignola P (2013b) Coexisting hydroxyl groups and H_2O molecules in
296 minerals: A single-crystal neutron diffraction study of eosphorite, $\text{MnAlPO}_4(\text{OH})_2 \cdot \text{H}_2\text{O}$. *Am*
297 *Mineral* 98:1297–1301.

298 Gatta GD, Jacobsen SD, Vignola P, McIntyre GJ, Guastella G, Abate LF (2014a) Single-
299 crystal neutron diffraction and Raman spectroscopic study of hydroxylherderite, $\text{CaBePO}_4(\text{OH},\text{F})$.
300 *Mineral Mag*, 78, 723-737.

301 Gatta GD, Vignola P, Meven M (2014b) On the complex H-bonding network in paravauxite,
302 $\text{Fe}^{2+}\text{Al}_2(\text{PO}_4)_2(\text{OH})_2 \cdot 8\text{H}_2\text{O}$: A single-crystal neutron diffraction study. *Mineral Mag* 78:841–850.

303 Gatta GD, Redhammer GJ, Vignola P, Meven M, McIntyre GJ (2015) Single-crystal neutron
304 diffraction and Mössbauer spectroscopic study of hureaulite, $(\text{Mn},\text{Fe})_5(\text{PO}_4)_2(\text{HPO}_4)_2(\text{H}_2\text{O})_4$. *Eur J*
305 *Mineral* 28:93-103.

306 Gatta GD, Fabelo Rosa OR, Fernandez-Diaz MT (2018a) On the crystal chemistry of the
307 wardite, $\text{NaAl}_3(\text{PO}_4)_2(\text{OH})_4 \times 2\text{H}_2\text{O}$. Institut Laue-Langevin (ILL, Grenoble): doi:10.5291/ILL-
308 DATA.5-11-430.

309 Gatta GD, Hålenius U, Bosi F, Cañadillas-Delgado L, Fernandez-Diaz MT (2018b) Minerals
310 in cement chemistry: a single-crystal neutron diffraction study of ettringite,
311 $\text{Ca}_6\text{Al}_2(\text{SO}_4)_3(\text{OH})_{12} \cdot 27\text{H}_2\text{O}$. *Am Mineral* (*in press*, DOI: <https://doi.org/10.2138/am-2019-6783>).

312 Heritsch H (1955) Die Raumgruppe von Wardit. *Tschermaks Min Petr Mitt* 5: 246-251.

313 Hurlbut CS (1952) Wardite from beryl mountain, New Hampshire. *Am Mineral* 37:849-852.

314 Kampf AR, Adams PM, Housley RM, Rossman GR (2014) Fluorowardite,
315 $\text{NaAl}_3(\text{PO}_4)_2(\text{OH})_2\text{F}_2 \cdot 2\text{H}_2\text{O}$, the fluorine analogue of wardite from the Silver Coin mine, Valmy,
316 Nevada. *Am Mineral* 99:804-810.

317 Larson AC (1967) Inclusion of secondary extinction in least-squares calculations. *Acta*
318 *Crystallogr* 23:664 – 665.

319 Lotti P, Gatta GD, Demitri N, Guastella G, Rizzato S, Ortenzi MA, Magrini F, Comboni D,
320 Guastoni A, Fernandez-Diaz MT (2017) Crystal-chemistry and temperature behavior of the natural
321 hydrous borate colemanite, a mineral commodity of boron. *Phys Chem Minerals* 45:405–422.

322 Mandarino JA, Sturman BD (1976) Kulanite, a new barium iron aluminum phosphate from the
323 Yukon Territory, Canada. *Can Mineral* 14:127-131.

324 Mandarino JA, Sturman BD, Corlett MI (1977) Penikisite, the magnesium analogue of
325 kulanite, from the Yukon Territory, Canada. *Can Mineral* 15:393-395.

326 Matthewman JC, Thompson P, Brown PJ (1982) The Cambridge Crystallography
327 Subroutine Library. *J Appl Crystallogr* 15:167-171.

328 Moore PB, Araki T, Merlino S, Mellini M, Zanazzi PF (1981) The arrojadite-dickinsonite
329 series, $\text{KNa}_4\text{Ca}(\text{Fe,Mn})^{2+}_{14}\text{Al}(\text{OH})_2(\text{PO}_4)_{12}$: crystal structure and crystal chemistry. *Am Mineral*
330 66:1034–1049.

331 Pouchou J-L, Pichoir F (1991) Quantitative analysis of homogeneous or stratified
332 microvolumes applying the method “PAP”. In: Heinrich KFJ, Newbury DE (eds) *Electron probe*
333 *quantitation*. Plenum Press, New York, 31-75.

334 Robertson BT (1982) Occurrence of epigenetic phosphate minerals in a phosphatic iron
335 formation, Yukon Territory. *Can Mineral* 20:177-187.

336 Roberts AC, Ansell HG, Jonasson IR, Grice JD, Ramik RA (1986) Rapidcreekite, a new
337 hydrated calcium sulfate-carbonate from the Rapid Creek area, Yukon Territory. *Can Mineral* 24:51-
338 54.

339 Robinson GW, Van Velthuisen J, Ansell HG, Sturman BD (1992) Mineralogy of the Rapid
340 Creek and Big Fish River area, Yukon Territory. *Min Rec* 23:1-47

341 Sears VF (1986) Neutron Scattering Lengths and Cross-Sections. In K. Sköld and D.L.
342 Price, Eds., *Neutron Scattering, Methods of Experimental Physics*, Vol. 23A, 521-550. Academic
343 Press, New York.

344 Sheldrick GM (2008) A short history of SHELX. *Acta Crystallogr A* 64:112-122.

345 Sheldrick GM (2014) SHELXL-2014. Programs for crystal structure determination and
346 refinement. University of Göttingen, Germany.

347 Steiner T (1998) Opening and narrowing of the water H-O-H angle by hydrogen-bonding
348 effects: Re-inspection of neutron diffraction data. *Acta Crystallogr B* 54:464-470.

349 Sturman BD, Mandarino JA (1976) Barićite, the magnesium analogue of vivianite, from the
350 Yukon Territory, Canada. *Can Mineral* 14:403-406.

351 Sturman BD, Dunn PJ (1984) Garyansellite, a new mineral from Yukon Territory. *Am Mineral*
352 69:207-209.

353 Sturman BD, Mandarino JA, Mrose ME, Dunn PJ (1981) Gormanite,
354 $\text{Fe}^{2+}_3\text{Al}_4(\text{PO}_4)_4(\text{OH})_6 \cdot 2\text{H}_2\text{O}$, the ferrous analogue of souzalite, and new data for souzalite. *Can Mineral*
355 19:381-387.

356 Vassilikou-Dova AB (1993) An EPR study of trivalent iron in wardite. *Appl Magn Reson*
357 5:25-29.

358 Wilkinson C, Khamis HW, Stansfield RFD, McIntyre GJ (1988) Integration of single-crystal
359 reflections using area multidetectors. *J Appl Crystallogr* 21:471-478.

360 Young FG, Robertson BT (1984) The Rapid Creek Formation: An Albian Flysch-Related
361 Phosphatic Iron Formation in Northern Yukon Territory. In: *The Mesozoic of Middle North America*,
362 D.F. Stott and D.J. Glass, eds. Canadian Society of Petroleum Geologists Memoir 9, 361-372.

363

364

365

366

367

368 Table 1. EPMA-WDS chemical analysis of wardite from Rapid Creek, Yukon, Canada. Average composition based on
 369 14 point analysis.
 370

Oxides	Wt%	e.s.d.
Na ₂ O	7.02	6.29-7.43
Al ₂ O ₃	37.84	36.53-39.31
SiO ₂	0.03	0.01-0.06
P ₂ O ₅	37.28	36.65-37.80
CaO	0.12	0.07-0.17
TiO ₂	0.10	0.04-0.15
MnO	0.02	0.01-0.06
Fe ₂ O ₃	0.93	0.50-1.45
H ₂ O	16.85	
Total	100.19	

Elements	a.p.f.u.
Na	0.91
Ca	0.01
Al	2.97
Fe ³⁺	0.05
Ti	0.01
Mn	0.00
P	2.10
H ⁺	7.48

Notes:

- Analysis calculated on the basis of 14 anions
- Fixed (OH)_{Σ=4}
- Fe₂O₃ calculated from FeO_{tot} obtained by microprobe analysis

The empirical formula of wardite results:
 $(\text{Na}_{0.91}\text{Ca}_{0.01})_{\Sigma=0.92}(\text{Al}_{2.97}\text{Fe}^{3+}_{0.05}\text{Ti}_{0.01})_{\Sigma=3.03}(\text{P}_{2.10}\text{O}_8)(\text{OH})_4 \cdot 1.74\text{H}_2\text{O}$

371
 372
 373
 374
 375
 376
 377
 378
 379
 380
 381
 382
 383

384 Table 2. Details of neutron data collection and refinement of wardite.

385
386
387
388
389
390
391
392
393
394
395
396
397
398
399
400
401
402
403
404
405
406
407
408
409
410
411

T (K)	20.0(5)
Crystal shape	Prism
Crystal volume (mm)	2 x 2 x 3
Crystal colour	Pale blue-green
Unit-cell parameters	$a = b = 7.0577(5)$ Å $c = 19.0559(5)$ Å
Chemical formula	NaAl ₃ (PO ₄) ₂ (OH) ₄ •2H ₂ O
Space Group	$P4_12_12$
Z	4
Radiation type	neutron
Wavelength (Å)	0.94602
Diffraction method	D19 four circle -ILL
Data-collection method	ω -scans
Max. 2θ (°)	122.25
	$-12 \leq h \leq +12$
	$-12 \leq k \leq +7$
	$-34 \leq l \leq +35$
Measured reflections	20478
Unique reflections	3109
Unique reflections with $F_o > 4\sigma(F_o)$	3106
Refined parameters	129
Extinction coeff.	0.0060(7)
R_{int}	0.0411
R_σ	0.0214
$R_I(F)$ with $F_o > 4\sigma(F_o)$	0.0219
$R_I(F)$ for all reflections	0.0221
$wR_2(F^2)$	0.0518
GooF	1.195
Residuals (fm/Å ³)	-0.68/+0.68
<i>Note:</i> Statistical parameters according to the Shelxl-2014 definition (Sheldrick 2008, 2014).	

412 Table 3. Refined fractional atomic coordinates and equivalent/isotropic displacement factors (\AA^2), based on the
 413 neutron structure refinement. U_{eq} is defined as one third of the trace of the orthogonalised U_{ij} tensor. All the sites show
 414 *s.o.f.s* of 100%.
 415
 416

<i>Site</i>	<i>x/a</i>	<i>y/b</i>	<i>z/c</i>	U_{eq}
P	0.14076(7)	0.36564(7)	0.34911(2)	0.00306(7)
A11	0.39588(11)	0.10694(11)	0.25770(4)	0.0029(1)
A12	0.10298(11)	0.10298(11)	0	0.0031(1)
Na	0.37371(11)	0.37371(11)	0.5	0.0063(1)
O1	-0.03785(7)	0.42506(7)	0.30966(3)	0.00483(7)
O2	0.29995(7)	0.51346(7)	0.33752(2)	0.00443(7)
O3	0.20513(7)	0.17351(7)	0.32071(3)	0.00497(7)
O4	0.09981(7)	0.35105(7)	0.42774(2)	0.00469(7)
O5	0.13341(7)	0.35260(7)	-0.03932(2)	0.00453(7)
O6	0.18718(7)	0.03209(7)	0.19138(3)	0.00585(7)
O7	0.40821(7)	0.34989(7)	0.21653(2)	0.00480(7)
H1	0.1264(2)	0.1027(2)	0.15197(6)	0.0178(2)
H2	0.1584(2)	-0.1030(2)	0.18760(7)	0.0199(2)
H3	0.0827(2)	0.3519(2)	-0.0860(1)	0.0232(2)
H4	0.5094(2)	0.3408(2)	0.18255(7)	0.0215(2)

417

418 Table 4. Refined displacement parameters (\AA^2) in the expression: $-2\pi^2[(ha^*)^2U_{11} + \dots + 2hka^*b^*U_{12} + \dots + 2klb^*c^*U_{23}]$
 419 and root-mean-square displacement amplitude (RMS , \AA), based on the neutron structure refinement of wardite.
 420

421
422

	U_{11}	U_{22}	U_{33}	U_{12}	U_{13}	U_{23}
P	0.0030(2)	0.0030(2)	0.0032(1)	0.0001(1)	-0.0001(1)	-0.0002(1)
A11	0.0030(2)	0.0028(2)	0.0031(2)	0.0001(2)	0.0000(2)	0.0002(2)
A12	0.0027(2)	0.0027(2)	0.0037(3)	-0.0002(2)	0.0002(2)	-0.0002(2)
Na	0.0062(2)	0.0062(2)	0.0067(3)	0.0001(3)	0.0000(2)	0.0000(2)
O1	0.0038(1)	0.0055(2)	0.0052(1)	0.0003(1)	-0.0008(1)	0.0012(1)
O2	0.0044(2)	0.0044(2)	0.0046(1)	-0.0012(1)	0.0001(1)	-0.0001(1)
O3	0.0054(2)	0.0038(2)	0.0058(2)	0.0004(1)	0.0010(1)	-0.0008(1)
O4	0.0046(1)	0.0058(2)	0.0037(1)	0.0003(1)	0.0003(1)	0.0002(1)
O5	0.0052(1)	0.0037(1)	0.0047(1)	0.0001(1)	-0.0003(1)	0.0001(1)
O6	0.0063(2)	0.0055(2)	0.0058(1)	-0.0003(1)	-0.0014(1)	0.0003(1)
O7	0.0051(1)	0.0038(1)	0.0055(1)	0.0001(1)	0.0007(1)	-0.0001(1)
H1	0.0201(4)	0.0182(4)	0.0151(3)	0.0020(3)	-0.0030(3)	0.0033(3)
H2	0.0241(5)	0.0119(3)	0.0236(5)	-0.0036(3)	-0.0035(4)	-0.0004(3)
H3	0.0365(7)	0.0197(5)	0.0133(4)	0.0020(5)	-0.0106(4)	-0.0014(3)
H4	0.0225(5)	0.0193(5)	0.0227(5)	0.0015(4)	0.0128(4)	0.0009(4)
	<i>RMS-min</i>	<i>RMS-mid</i>	<i>RMS-max</i>	<i>max/min</i>		
P	0.05405	0.05430	0.05762	1.066		
A11	0.05175	0.05428	0.05644	1.091		
A12	0.05029	0.05230	0.06180	1.229		
Na	0.07756	0.07937	0.08188	1.056		
O1	0.05591	0.06932	0.08093	1.448		
O2	0.05612	0.06734	0.07493	1.335		
O3	0.05677	0.07116	0.08144	1.435		
O4	0.05978	0.06772	0.07694	1.287		
O5	0.06112	0.06750	0.07285	1.192		
O6	0.06802	0.07356	0.08673	1.275		
O7	0.06180	0.06797	0.07727	1.250		
H1	0.10714	0.14260	0.14685	1.371		
H2	0.10362	0.14534	0.16661	1.608		
H3	0.09549	0.13966	0.20222	2.118		
H4	0.09881	0.13837	0.18875	1.910		

423
424
425
426
427
428
429
430
431
432
433
434
435
436

437
438
439
440

Table 5. Relevant bond distances (Å) and angles (°) based on the neutron structure refinement.

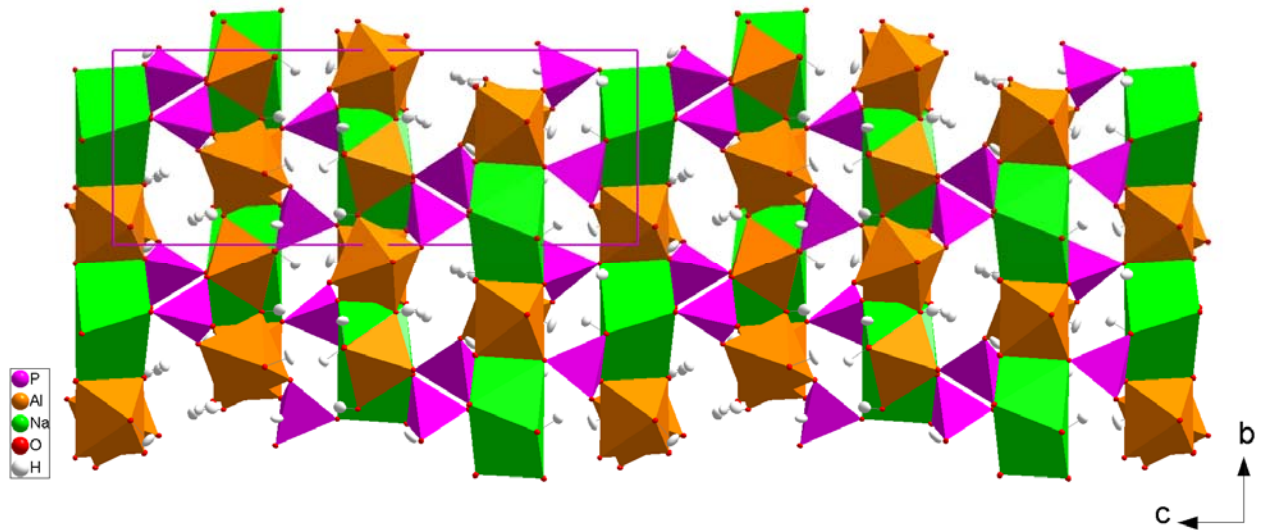
P - O1	1.5265(7)	O1 - P - O2	110.10(4)	O5-H3	0.959(1)
P - O2	1.5490(7)	O1 - P - O3	108.34(4)	O5-H3*	0.986
P - O3	1.5291(7)	O1 - P - O4	110.18(4)	O5-H3...O1	139.9(1)
P - O4	1.5295(5)	O2 - P - O3	109.35(4)	O5...O1	3.347(1)
		O2 - P - O4	108.79(4)	H3...O1	2.556(1)
Al1 - O1	1.8661(9)	O3 - P - O4	110.07(4)	O5-H3...O6	148.5(1)
Al1 - O3	1.8641(9)			O5...O6	3.205(1)
Al1 - O4	1.9165(9)	O1 - Al1 - O3	176.37(5)	H3...O6	2.347(1)
Al1 - O5	1.9047(9)	O1 - Al1 - O4	88.48(4)		
Al1 - O6	2.0114(9)	O1 - Al1 - O5	92.57(4)	O6-H1	0.998(1)
Al1 - O7	1.8876(9)	O1 - Al1 - O6	89.72(4)	O6-H1*	1.013
		O1 - Al1 - O7	85.43(4)	O6-H1...O2	174.4(1)
Al2 - O2 x 2	1.9105(6)	O3 - Al1 - O4	95.16(4)	O6...O2	2.613(1)
Al2 - O5 x 2	1.9265(9)	O3 - Al1 - O5	87.44(4)	H1...O2	1.617(1)
Al2 - O7 x 2	1.8983(9)	O3 - Al1 - O6	86.68(4)		
		O3 - Al1 - O7	94.13(4)	O6-H2	0.978(1)
Na - O4 x 2	2.3788(8)	O4 - Al1 - O5	91.39(4)	O6-H2*	0.996
Na - O1 x 2	2.4756(7)	O4 - Al1 - O6	173.67(4)	O6-H2...O5	160.1(1)
Na - O6 x 2	2.5659(10)	O4 - Al1 - O7	95.26(4)	O6...O5	2.852(1)
Na - O3 x 2	2.7199(8)	O5 - Al1 - O6	82.63(4)	H2...O5	1.913(1)
		O5 - Al1 - O7	173.00(5)	H1-O6-H2	110.0(1)
		O6 - Al1 - O7	90.64(4)		
				O7-H4	0.966(1)
		O2 - Al2 - O2	177.74(5)	O7-H4*	0.989
		O2 - Al2 - O5	92.78(4)	O7-H4...O3	160.5(1)
		O2 - Al2 - O5	85.58(3)	O7...O3	3.373(1)
		O2 - Al2 - O7	89.83(4)	H4...O3	2.447(1)
		O2 - Al2 - O7	91.74(3)	O7-H4...O4	137.9(1)
		O5 - Al2 - O5	86.98(4)	O7...O4	3.231(1)
		O5 - Al2 - O7	90.70(3)	H4...O4	2.449(1)
		O5 - Al2 - O7	174.75(4)		
		O7 - Al2 - O7	91.98(4)		

* Bond distance corrected for "riding motion" following Busing and Levy (1964)

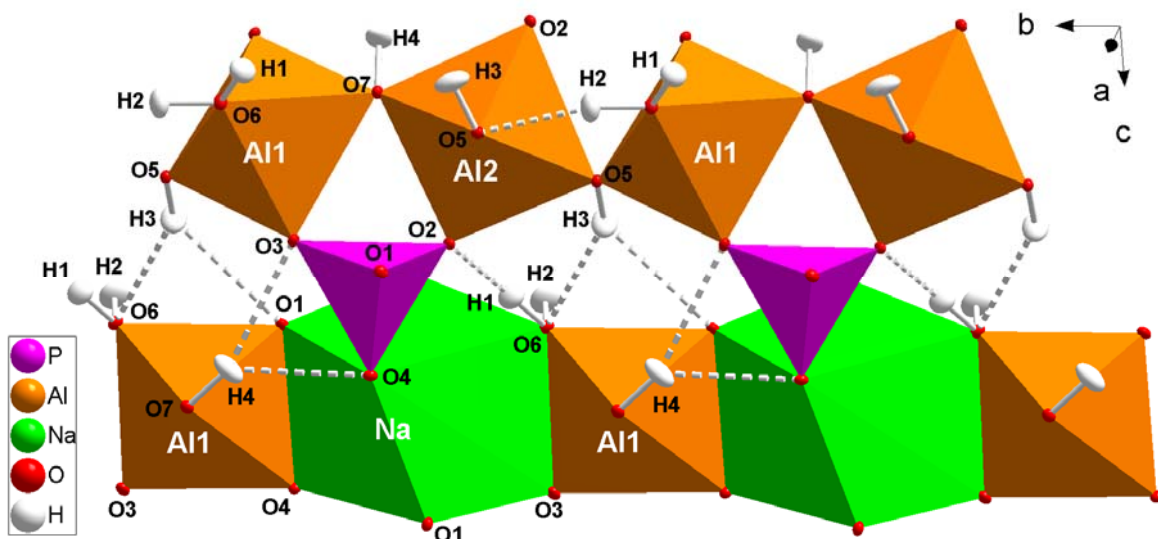
441
442
443
444
445
446
447
448
449
450
451
452
453
454
455
456

457
458
459
460
461
462
463

Figure 1. Two views of the crystal structure of wardite based on the neutron structure refinement of this study (intensity data collected at 20 K). Displacement ellipsoid probability factor: 50%.



464
465



466
467
468
469
470
471
472
473
474
475
476

477 Figure 2. Difference-Fourier maps of the nuclear density (xy sections, x horizontal; $z \sim 0.15$ for the H1 map, $z \sim 0.19$ for the H2 map, $z \sim -0.09$ for the H3 map, $z \sim$
478 0.18 for the H4 map) calculated with coefficients $F_o - F_c$ and phased by F_c . The F_c were calculated from a structural model without the H sites. Minima,
479 ascribable to the missing H sites (as H has negative neutron scattering length) are visible. Color bar unit: $\text{fm}/\text{\AA}^3$.
480

